Development of a Micromachined Differential Type Resonant Accelerometer and Its Performance

Chul Hyun*, Jang-Gyu Lee*, Tae-Sam Kang**, Sang-Kyung Sung***, Seon-Ho Seok*, and Kuk-Jin Chun*

* Department of Electrical Engineering, Seoul National University, Seoul, Korea
(Tel : +82-2-872-8190; E-mail: hyun@asrignc3.snu.ac.kr)
**Department of Aerospace Engineering, Konkuk University, Seoul, Korea
(Tel : +82-2-450-3544; E-mail: tskang@konkuk.ac.kr)
***Telecommunication R&D Center, Samsung Electronics co. ltd. , Suwon, Korea
(Tel : +82-31-279-5839; E-mail: s.sung@samsung.com)

Abstract: This paper presents the differential type resonant accelerometer (DRXL) and its performance test results. The DRXL is the INS grade, surface micro-machined sensor. The proposed DRXL device produces a differential digital output upon an applied acceleration, and the principle is a gap-dependent electrical stiffness variation of the electrostatic resonator with torsion beam structures. Using this new operating concept, we designed, fabricated and tested the proposed device. The final device was fabricated by using the wafer level vacuum packaging process. To test the performance of the DRXL, a nonlinear self-oscillation loop is designed using describing function technique. The oscillation loop is implemented using discrete electronic elements. The performance test of the DRXL shows that the sensitivity of the accelerometer is 12 Hz/g and its long term bias stability is about 2 mg(1 σ). The turn on repeatability, bandwidth, and dynamic range are 4.38 mg, 100 Hz, and $\pm$ 70g, respectively.

Keywords: Resonant type accelerometer, Micromachining, Self-sustained oscillation loop.

1. INTRODUCTION

Recently, a novel resonant accelerometer of navigation-grade performance, named ACRC-RXL, has been developed using mixed micromachining processes[1-3].

A resonant sensor has many advantages over the conventional capacitive type: wide dynamic range, quasi-digital nature of the output signal, and the inherent continuous self-test capability. The quartz-based resonant accelerometers have been used for navigation-grade sensing [4,8], and recently, some research groups have announced several kinds of MEMS based resonant accelerometers [5,6,7,9].

The working principle of the DRXL is just like conventional pendulous accelerometer and uses resonators to pick off the differential gap change induced by the applied acceleration. So it is less sensitive to the internal residual stress and the sensitivity to the acceleration can be doubled due to its differential characteristics. Furthermore, it uses surface micromachining processes which has been proven as a manufacturable technology. Thus the DRXL can be easily mass produce with low cost.

In the following, the brief introduction of the DRXL, design of the self-sustained oscillation loop to maintain resonance and its implementation, the performance test results are presented.

2. STURCTURE AND OPERATING PRINCIPLE

2.1 Structure

The basic structure of DRXL is shown in Fig. 1. It consist of the outer gimbals(*M1, M2*) which is the acceleration sensitive structure, the inner resonator(M_r) whose resonance frequency can be change by a variable gap, and bottom plate electrode*(S,D,T)* which apply the electrical bias to the resonator.

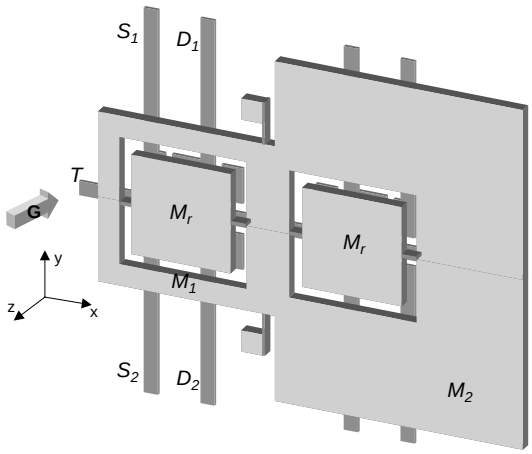

Fig. 1 Schematic diagram of the proposed differential resonant accelerometer (DRXL)

A resonant accelerometer, which utilizes an electrostatic stiffness changing effect, has special features of high sensitivity, electrical tunability, and very simple fabrication process[7]. But this kind of parallel plate resonant structure has some drawbacks of non-linearity, and difficulty in controlling the resonant vibration mode within the stable region, because the vibrating mode is parallel to the input acceleration axis. In this paper, we decoupled the acceleration sensitive structure and gap sensitive resonator using separated torsion beams as shown in Fig. 1.

In this scheme, the external acceleration(*G*) produces the average gap variation between the resonant vibrating mass and the bottom electrodes because of the asymmetric mass distribution. And these gap variation changes the effective stiffness of the resonator and the resultant resonant frequency as well. Because of the complementary gap variations, the resultant resonant frequency outputs are differential.

2.2 Operating principle

When the external acceleration is applied to the DRXL, as shown in the Fig. 2, the outer mass(*M1, M2*) is tilted due to the asymmetric mass distribution as follows :

$$\theta_y = \frac{\tau_G}{k_{eff_y}} = \frac{(M_1 + M_2)\cdot G \cdot R_G}{k_{m_y} - \dfrac{2R_T{}^2 \cdot \varepsilon \cdot A_T \cdot V_T{}^2}{d_0^3}} \tag{1}$$

where θ_y , τ_G , k_{m_y} , k_{eff_y} , R_G , R_T , A_T , V_T , and d_0 represent tilt angle of the outer mass, the applied torque due to the external acceleration and mass asymmetry, the mechanical elastic stiffness of the supporting spring of the outer gimbal, the difference of k_{m_y} and the electrical stiffness of the outer gimbal, the distance between rotation axis and the mass center of the outer gimbal, the distance between rotation axis and the center of the inner resonator plate, the area of the tuning electrode, the applied tuning voltage, and the nominal gap between outer mass plate and bottom plate, respectively.

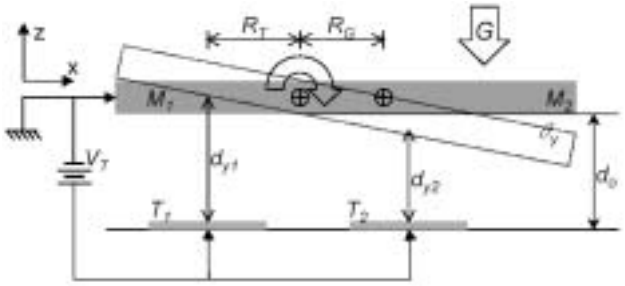

Fig. 2 Schematic for outer gimbal

The schematic diagram for the one side inner resonator is given in Fig. 3. Note that the resonator parameter for the other side is the same one except that the average gap between the upper resonator plate and the bottom plate is different when external acceleration is applied.

The plant dynamics of the resonator is given as

$$\tau_{eff_x} = I_x\ddot{\theta}_x + D_x\dot{\theta}_x + k_{eff_x}\theta_x \tag{2}$$

where τ_{eff_x} is the torque applied to the resonator and I_x , θ_x , D_x , and k_{eff_x} represent inertia, tilt angle, damping coefficient, and net elastic coefficient of the resonator, respectively. The τ_{eff_x} is given as the difference of the electrical torque from the applied mechanical torque :

$$\tau_{eff_x} = \tau_{m_x} - \tau_{e_x} = \theta_x \cdot k_{eff_x} = \theta_x \cdot \left(k_{m_x} - \frac{2R_S{}^2 \cdot \varepsilon \cdot A_S \cdot V_S{}^2}{d_x^3} \right) \tag{3}$$

where k_{m_X} , R_S , ε , A_S , V_S and d_x represent mechanical elastic coefficient, the distance between center of resonator and that of sensing electrode, dielectric constant, the area of the sensing electrode, the applied bias voltage, and the gap between upper resonator plate and bottom plate.

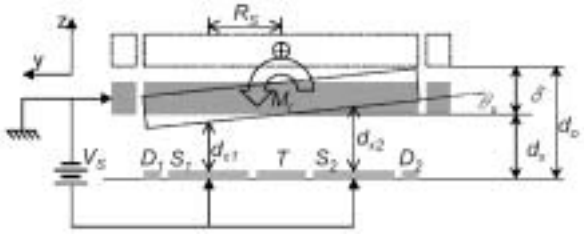

Fig. 3 Schematic for inner resonator.

Then the resonance frequency is approximately given as

$$f_{r_x} = \frac{1}{2\pi}\cdot\sqrt{\frac{k_{eff_X}}{I_x}} = \frac{1}{2\pi}\cdot\sqrt{\frac{1}{I_x}\left(k_{m_X} - \frac{2R_S{}^2 \cdot \varepsilon \cdot A_S \cdot V_S{}^2}{d_x^3}\right)} \tag{4}$$

Note that the effective stiffness (k_{effx}) of this electro-mechanically-biased resonator can be changed by a variable gap (d_x).

2.3 Resonant Property

Fig. 4 is the MATLAB simulation results. It shows that its output is symmetrical around zero input and linear in the small input region which is due to differential out measurement. The G sensitive resonant frequency of each resonator has a large non-linearity but the resultant linearity is fairly improved by taking the frequency differences as output. The electrostatic stiffness changing effect of the proposed accelerometer has a merit that its nominal resonant frequency can be tuned electrically, so we can finely adjust the sensitivity of the resonant accelerometer at the final stage. And this is a very useful method for removing the effect of the fabrication error.

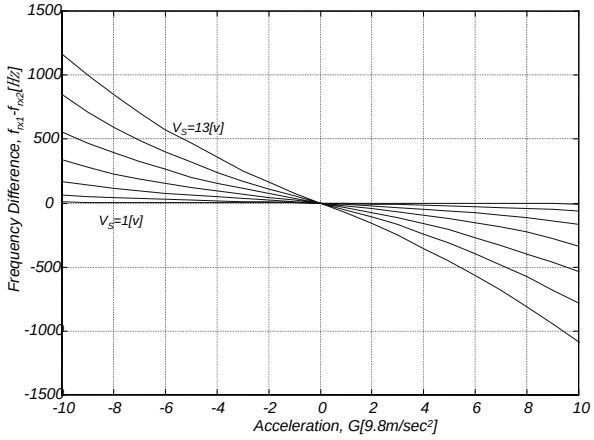

Fig. 4 Frequency differences vs. applied acceleration, G

3. OSCILLATION LOOP DESIGN

The oscillation loop is designed using an analytical result based on the describing function method, since the fundamental principle of harmonic balance simplifies the nonlinear system analysis. Furthermore, the quasi-linearized describing function method can provide the stability and optimality criterion through the strict theoretical development. In this paper, we briefly introduce the theoretical result to construct an efficient and stable self-sustained oscillation loop,

which is applied to both sub-resonators of DRXL.

The configuration for the nonlinear feedback system is given in the Fig. 5.

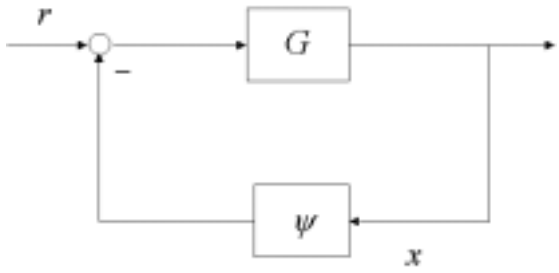

Fig. 5 Nonlinear feedback system for DRXL.

The G(s) is the transfer function given by Eq. (2) and the ψ is the feedback nonlinearity that is inserted to keep resonant oscillation. We used amplifier with saturation and phase shifter for the nonlinear part. The gain of the amplifier and the phase shift are chosen so that the oscillation loop is robustly maintained and the undesired harmonic terms are minimized. Note that the nonlinearity is designed to be single-valued, odd symmetric, and sector bounded as follows

$$c_1(x_A - x_B) \le \left[\psi(x_A) - \psi(x_B)\right] \le c_2(x_A - x_B) \tag{5}$$

for all real variables x_A and x_B where $x_A \ge x_B$.

Now the loop equation in Fig. 6 is given as

$$x = -G\psi(x) \tag{6}$$

Also, due to the nonlinearity conditions, the loop solution of Eq. (6) can be assumed to be half-wave symmetric, i.e.

$$x(t) = a_1 \sin \omega t \quad (:= x_1(t)) + \sum_{k>1,odd}^{\infty} b_k \sin k\omega t \tag{7}$$

where the right-hand side is sum of a dominant sinusoid denoted by $x_1(t)$ and its higher-order harmonics. Then the describing function technique simplifies the nonlinear loop equation in Eq. (6) into the first-order harmonic balance, namely

$$1 + G(j\omega)\Psi_N(a_1)\, e^{j\phi} = 0 \tag{8}$$

where $\Psi_N(\cdot)$ denotes the describing function of $\psi(x)$ without the phase delay.

The phase delay ϕ can be used to define the limit cycle point. The sector higher bounded c_2 is set to 5×10^6 so that Eq. (8) has a nontrivial solution, i.e., a limit cycle to exist, and c_1 is set to zero for convenience, usually.

With the predefined parameters, the oscillation loop can be further elaborated to obtain the design factor of optimally undistorted sinusoid. This can be shown by deriving the inequality that the ratio between the magnitude of higher order terms and the amplitude of dominant sinusoid is given by

$$\left\|\eta(x_1)\right\| \le \frac{\frac{c_2 - c_1}{2}}{\left|\frac{c_1 + c_2}{2} + G^{-1}(j3\omega)\right| - \frac{c_2 - c_1}{2}} \cdot \left\|x_1\right\| \tag{9}$$

which can be referred to[10]. With this loop design criterion, the phase shift ϕ is used to minimize the bound of $\|\eta(x_1)\|$ in Eq. (9). The minimal higher order terms with regards to principal amplitude is numerically obtained when ϕ is near $3\pi/2$.

4. IMPLEMENTATION

After dicing the bonded wafer and attaching the each packaged DRXL die to a 16pin DIP ceramic holder, the device is obtained and used to sense the acceleration as in the Fig. 6. Note that the sensor element is the tiny device placed on the lower middle part of the signal processing electronics shown in the Fig. 6. To convert the gap change due to acceleration input to voltage difference, a charge amplifier circuit, shown in Fig. 7, is used.

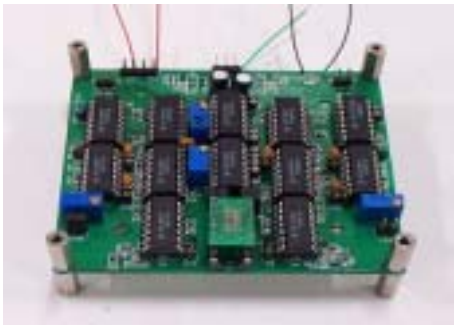

Fig. 6 Photographs of the DRXL chip and its signal processing electronics

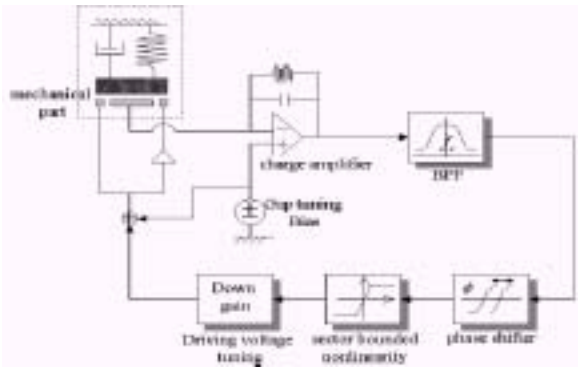

Fig 7. Circuit diagram for the feedback system.

The feedback oscillation loop is implemented using discrete element as shown in Fig. 7. To detect minute change of the capacitance due to the gap variation according to the applied acceleration, a precision charge amplifier is devised which can measure an electrical capacitance of sub-femto farads.

Then the nonlinearity in Fig. 7 is realized by cascading phase shifter and Schmitt trigger. The proper phase shift is obtained by tuning a resistor in the phase-shift circuit. The sector-bounded saturated amplifier is obtained by setting the feedback nodes of the Schmitt trigger circuit, with proper slew rate, to be open. After down gaining the saturation output, it is added to the gap tuning bias and then fed back to the driving electrode of mechanical structure.

5. PERFORMANCE TEST

Fig. 8 shows the resonant characteristic of the DRXL. It can be seen that the nominal resonant frequency is about 12.532kHz, signal to noise ratio (SNR) is about 25dB, and the quality factor is about 250.

After the phase and gain of the feedback components are fixed, the oscillation loop activates a resonance with the help of initial white noise in the driving voltage. The warming time to resonance is less than 30 ms, which is near to the settling time.

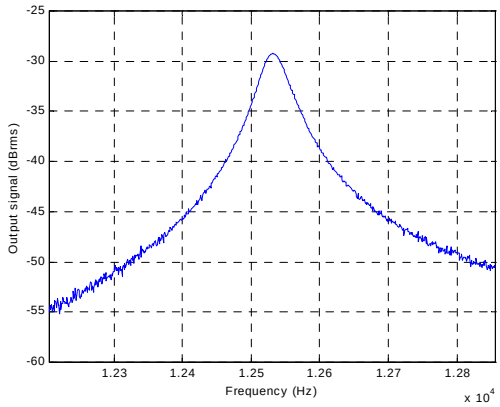

Fig. 8 Resonant characteristic of the DRXL.

Fig. 9 shows an output of the constructed loop in the frequency domain. From Fig. 9, a *Q*-factor of 40000 is obtained, which shows quite an improved resolution compared to that of the sensing device only.

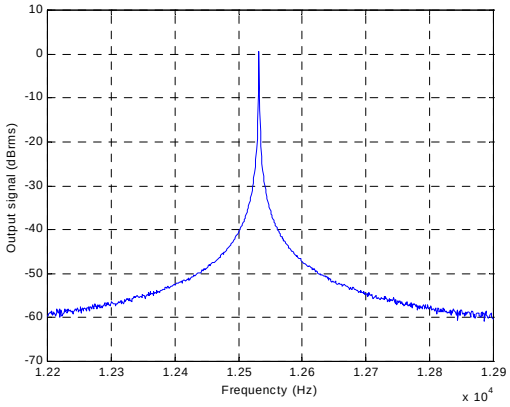

Fig. 9 Output characteristics of the DRXL with self-oscillation loop.

The acceleration sensitivity was measured by tumble test with applying 2.5[V] on the sensing electrode, and the result is shown in Fig. 10. The nominal resonant frequency is 12,532[㎐] and the sensitivity is 12[㎐/g]. The sensitivity is obtained using only one side resonator. Noting that the other side resonator responses complementary, the sensitivity can be doubled when the both resonators are used.

Fig. 11 shows the static bias drift of the DRXL when zero gravity is applied. The obtained equivalent bias drift is about 2 mg of 1 σ standard deviation from output data for 10 hours. And Fig. 12 represents a step response of oscillating amplitude, which shows bandwidth is about 100Hz

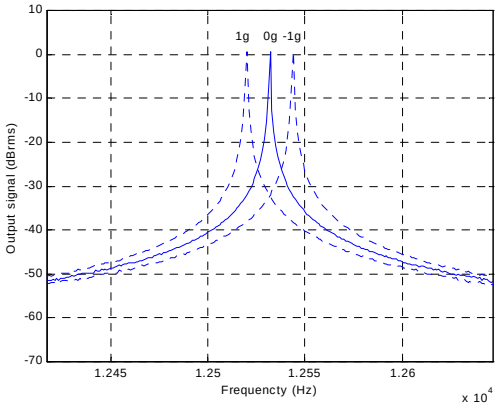

Fig. 10 Tumble test result of the DRXL.

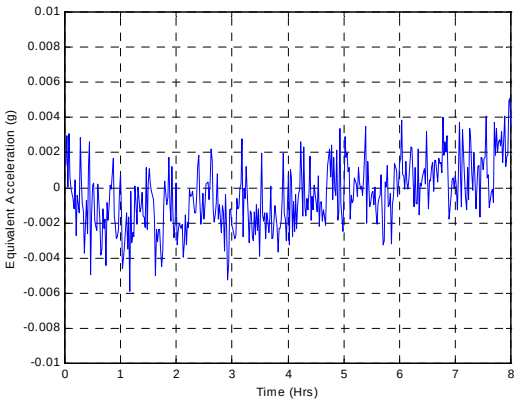

Fig. 11 Output bias stability of DRXL.

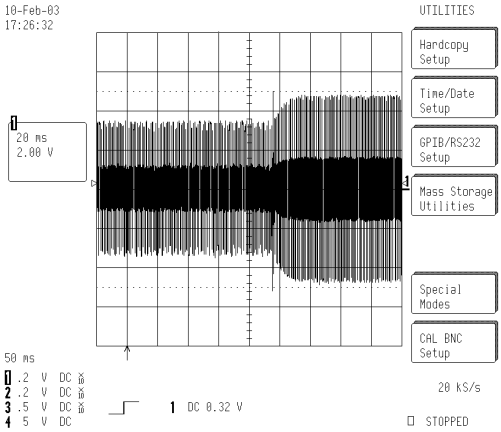

Fig. 12 Step response in time domain

Fig. 13 shows turn on/off repeatability of 4.38mg at 12332Hz, which is the main source of the accelerometer's random bias noise. Random Bias acquired from 7 repeated trials of 2 hours 'On' time and 1 hours interval time. X axis is trial number and Y axis is the output frequency. Equivalent bias is acquired by using DRXL's sensitivity.

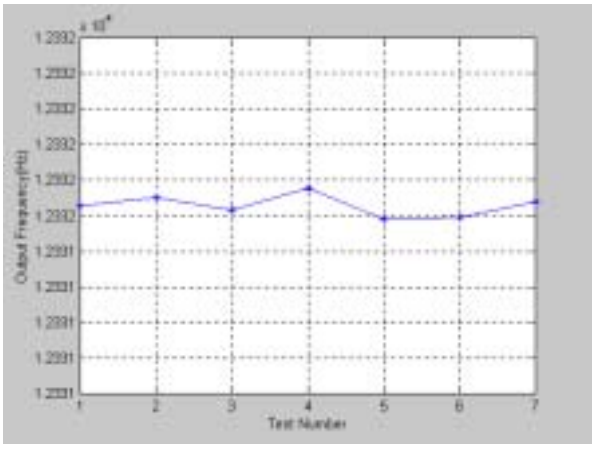

Fig. 13 Turn On/Off repeatability test

6. CONCLUSION

A differential resonant accelerometer, which utilizes the electrostatic stiffness changing effect of an electrostatic torsional actuator, is proposed. This accelerometer has differential resonant structures, which can be used to improved the linearity and sensitivity. The surface micro-machined sensor wafer was fabricated by epitaxially grown and polished thick polysilicon process. The self-oscillation loop is designed using describing function technique and implemented using discrete electronic devices. The performance tests show that the bias stability is about 2 mg with 12 Hz/g sensitivity, 100Hz bandwidth, 4.38mg turn on repeatability, and ± 70g dynamic range, which demonstrates the feasibility of high quality and low cost MEMS accelerometer.

ACKNOWLEDGEMENTS

This work was supported by Agency for Defense Development through Automatic Control Research Center in Seoul National University. The authors sincerely appreciate that the device was fabricated by Microsystems Technology Center in Seoul National University.

REFERENCES

[1] B. L. Lee, C. H. Oh, Y. S. Oh and K. Chun, "A novel resonant accelerometer; variable electrostatic stiffness type," *Proceedings of International Conference on Solid State Sensors and Actuators*, 1999, Sendai, pp.1546-1549.

[2] L. Lee, C. H. Oh, S. Lee, Y. S. Oh and K. Chun, "A vacuum packaged differential resonant accelerometer using gap sensitive electrostatic stiffness changing effect," *Proceedings of the 13th International Conference on MEMS*, January 2000, Miyazaci, pp.352 –357.

[3] S. Sung, J. G. Lee, T. Kang and J. W. Song, "Design and analysis of nonlinear feedback loop for a resonant accelerometer," *Proceedings of European Control Conference (ECC 2001)*, September 2001, Porto, pp.1906-1911.

[4] B. L. Norling, "Superflex: a synergitic combination of vibrating beam and quartz flexure accelerometer," *Journal of the Institute of Navigation*, Vol.34, No.4, 1988, pp. 337-353.

[5] D. W. Burns, et al., "Resonant microbeam accelerometer," *International Conference on Solid-State Sensors and Actuators (Transducers `95)*, pp.659-662.

[6] Trey A. Rossig, et al., "Surface-Micromachined Resonant Accelerometer," *International Conference on Solid State Sensors and Actuators (Transducers '97)*, pp.869-862.

[7] M. A. Meldrum, "Application of vibration beam technology to digital acceleration measurement," *Sensor and Actuators*, Vol. A21-A23, 1990, pp377-380.

[8] T. V. Rozhart, et al., "An inertial-grade, micromachined vibrating beam accelerometer," *Eighth International Conference on Solid-State Transducers and Actuators (Transducers `95)*, 1995, pp.659-662.

[9] Yoshiteru Omura, et al., "New Resonant Accelerometer Based on Rigidity Change," *International Conference on Solid State Sensors and Actuators (Transducers `97)*, pp.855-858.

[10] S. Sung, *A Feedback Loop Design for MEMS Resonant Accelerometer Using a Describing Function Technique*, Ph.D. Thesis, Seoul National University, Feb 2003.